IL NUOVO CIMENTO Vol. 28 C, N. 1 Gennaio-Febbraio 2005
DOI 10.1393/ncc/i2005-10022-8

Langmuir cells and mixing in the upper ocean

S. Carniel(1)(*), M. Sclavo(1), L. H. Kantha(2) and C. A. Clayson(3)

(1) *CNR, ISMAR - San Polo 1364, I-30125, Venice, Italy*

(2) *Department of Aerospace Engineering Sciences, University of Colorado Boulder (CO), USA*

(3) *Department of Meteorology, Florida State University - Tallahassee (FL), USA*

(ricevuto il 15 Febbraio 2005; revisionato il 7 Marzo 2005; approvato l'11 Marzo 2005)

Summary. — The presence of surface gravity waves at the ocean surface has two important effects on turbulence in the oceanic mixed layer (ML): the wave breaking and the Langmuir cells (LC). Both these effects act as additional sources of turbulent kinetic energy (TKE) in the oceanic ML, and hence are important to mixing in the upper ocean. The breaking of high wave-number components of the wind wave spectrum provides an intense but sporadic source of turbulence in the upper surface; turbulence thus injected diffuses downward, while decaying rapidly, modifying oceanic near-surface properties which in turn could affect the air-sea transfer of heat and dissolved gases. LC provide another source of additional turbulence in the water column; they are counter-rotating cells inside the ML, with their axes roughly aligned in the direction of the wind (Langmuir I., *Science*, **87** (1938) 119). These structures are usually made evident by the presence of debris and foam in the convergence area of the cells, and are generated by the interaction of the wave-field–induced Stokes drift with the wind-induced shear stress. LC have long been thought to have a substantial influence on mixing in the upper ocean, but the difficulty in their parameterization have made ML modelers consistently ignore them in the past. However, recent Large Eddy Simulations (LES) studies suggest that it is possible to include their effect on mixing by simply adding additional production terms in the turbulence equations, thus enabling even 1D models to incorporate LC-driven turbulence. Since LC also modify the Coriolis terms in the mean momentum equations by the addition of a term involving the Stokes drift, their effect on the velocity structure in the ML is also quite significant and could have a major impact on the drift of objects and spilled oil in the upper ocean. In this paper we examine the effect of surface gravity waves on mixing in the upper ocean, focusing on Langmuir circulations, which is by far the dominant part of the surface wave contribution to mixing.

(*) E-mail: sandro.carniel@ismar.cnr.it

Oceanic ML models incorporating these effects are applied to an observation station in the Northern Adriatic Sea to see what the extent of these effects might be. It is shown that the surface wave effects can indeed be significant; in particular, the modification of the velocity profile due to LC-generated turbulence can be large under certain conditions. However, the surface wave effects on the bulk properties of the ML, such as the associated temperature, while significant, are generally speaking well within the errors introduced by uncertainties in the external forcing of the models. This seems to be the reason why ML models, though pretty much ignoring surface wave effects until recently, have been reasonably successful in depicting the evolution of the mixed layer temperature (MLT) at various timescales.

PACS 92.10.Fj – Dynamics of the upper ocean.
PACS 92.10.Lq – Turbulence and diffusion.
PACS 92.10.Kp – Sea-air energy exchange processes.
PACS 07.05.Tp – Computer modeling and simulation.

1. – Introduction

There has been significant progress in the study of wave-turbulence interactions in recent years (for example, [1-3]), which is a welcome development since such interactions have long been ignored in dealing with upper ocean mixing and wind wave evolution. Other recent progresses concerning surface gravity waves and mixing in the upper ocean have been forwarded by oceanic ML modelers such as [4] and [5]. These effects include those due to wave breaking, injecting turbulence directly into the upper few meters of the water column, and those due to organized Langmuir circulations, which enhance turbulence production throughout the water column in addition to introducing cellular motions in the vertical. In ref. [4] wave-breaking effects are studied, while in [5] the effects of both wave breaking and LC are investigated, though without carrying out a detailed parametric study of the effect of Langmuir TKE production on ML dynamics. It is our intention here to do so, while applying the model to the Adriatic Sea.

Langmuir circulation arises from the interaction of the wind-driven shear with the Stokes drift of the surface waves [6]. The mean momentum equations are modified by the appearance of a vortex force term as well as the modification of the Coriolis term by the Stokes drift ([7], see also [5]). It is the latter that affects the velocity structure in the upper ocean. The mean momentum equations with LC are written as

$$\frac{\partial U_j}{\partial t} + \frac{\partial}{\partial x_k}\left(U_k U_j\right) + \left(\varepsilon_{jkl} f_k\right)\left(U_l + V_{Sl}\right) = -\frac{1}{\rho_0}\frac{\partial \Pi}{\partial x_j} - g_j \beta \Theta - \frac{\partial}{\partial x_k}\left(\overline{u_k u_j}\right) + \left(\varepsilon_{jpl} V_{Sp} \Omega_l\right) , \tag{1}$$

where U and u represent, respectively, the mean and fluctuating quantities for velocity, Θ the mean temperature, g the gravity acceleration, and β the thermal expansion coefficient. The quantity $\Omega_l = \varepsilon_{lmn}(\partial U_n/\partial x_m)$ is the vorticity, and Π the generalized pressure that includes the Stokes drift contribution, and is given by

$$\Pi = p + \frac{\rho_0}{2}\left[\left(U_i + V_{Si}\right)\left(U_i + V_{Si}\right) - V_{Si} V_{Si}\right] , \tag{2}$$

where p is the pressure and ρ_0 a reference density. The quantity V_{Si} (note that $V_{S3} = 0$) is the Stokes drift velocity due to the surface gravity wave, whose magnitude is given by

$$|V_S| = (V_{Si}V_{Si})^{1/2} = V_{S0}e^{2kz} = C\,(ka)^2\,e^{2kz}\,, \tag{3}$$

where V_{S0} is the Stokes drift velocity magnitude at the surface, C is the wave phase speed, k is the wave number and a is the wave amplitude. The vortex force term acts like a buoyancy term in the vertical momentum equation. For more details, see [7].

It is rather self-evident that it is difficult to incorporate the influence of Langmuir cellular circulation in the vertical in 1D models. However, the additional production of TKE in the ML by LC can be taken into account by incorporating additional production terms in both the TKE and the length scale equations. For the $q^2 - q^2 l$ model, the governing equations become [5]

$$\begin{aligned}\frac{D}{Dt}\left(q^2\right) - \frac{\partial}{\partial z}\left[q\ell S_q \frac{\partial}{\partial z}\left(q^2\right)\right] &= 2(P + B - \varepsilon) = -2\overline{uw}\left(\frac{\partial U}{\partial z} + \frac{\partial u_S}{\partial z}\right) - \\ &- 2\overline{vw}\left(\frac{\partial V}{\partial z} + \frac{\partial v_S}{\partial z}\right) + 2\beta g\overline{w\theta} - 2\frac{q^3}{B_1\ell}\,,\end{aligned} \tag{4}$$

$$\begin{aligned}\frac{D}{Dt}\left(q^2\ell\right) - \frac{\partial}{\partial z}\left[q\ell S_\ell \frac{\partial}{\partial z}\left(q^2\ell\right)\right] &= -E_1\ell\left(-\overline{uw}\frac{\partial U}{\partial z} - \overline{vw}\frac{\partial V}{\partial z}\right) + \\ &+ E_6\ell\left(-\overline{uw}\frac{\partial u_S}{\partial z} - \overline{vw}\frac{\partial v_S}{\partial z}\right) + E_3\left(\beta g\overline{w\theta}\right) - E_2\frac{q^3}{B_1}\left[1 + E_4\left(\frac{\ell}{\kappa\ell_w}\right)^2\right],\end{aligned} \tag{5}$$

where w and θ represent the fluctuating quantities for the vertical velocity and temperature, u_s, v_s are the components of the Stokes drift velocity V_S. The values of the closure constants are $S_q = 0.41$, $S_l/S_q = 3.74$, $E_1 = 1.8$, $E_2 = 1.0$, $E_3 = 1.0$, $E_4 = 4.88$ and $E_6 = 4.0$. Note that E_3 should have a higher value under stable stratification, but a similar effect is achieved by imposing a limit on the length scale via the condition $Nl/q < 0.53$, where N is the buoyancy frequency (see [8]).

Modifications to the K-ε model (see [9, 10]) are similar and the corresponding governing equations are given in [10].

The main effect is therefore the introduction of additional TKE into the water column (note the presence of production terms due to LC in both the TKE and length scale equations of the two-equation turbulence models), unlike wave breaking which injects turbulence only near the air-sea interface. This is due to the fact that wave breaking only affects a depth of the order of the wave amplitude, whereas the depth of influence of the Stokes drift, and hence the Langmuir circulation, scales with the wavelength. As the turbulence injected into the water column by wave breaking decays rapidly away from the surface, its effects can be expected to be confined to near-surface layers, whereas Langmuir production of TKE can be expected to enhance the TKE and mixing in the entire water column. Nevertheless, the extent of contribution of Langmuir production depends very much on the vertical shear of the Stokes drift velocity in the water column. Thus, the likely non-dimensional parameters of interest for the case of monochromatic surface gravity wave are kD (where k is the wave number and D is the mixed layer depth (MLD)) and V_{S0}/u_*, where V_{S0} is the Stokes drift velocity magnitude at the surface — see eq. (3)— and u_* is the friction velocity. The Langmuir number defined by [7] as $La = \left(\frac{u_*}{V_{S0}}\right)^{1/2}$ can be used as an alternative to the latter parameter.

For a wave spectrum, the effective values of k and V_{S0} must be derived from the spectral shape. When wave breaking is present, the TKE at the surface is enhanced: $k = k_0(1+m)^{2/3}$ where $m = m(A)$ is a function of wave age $A = C_p/u_*$, C_p being the peak phase speed. For fully developed waves, [5] used $m = 66.6$; the large value of m means that the errors in ML properties resulting from the assumption of fully developed wave field are usually negligible [2].

Wave breaking acts independent of the ambient turbulence in the ML, whereas the presence of the Reynolds stress is essential for converting wave-induced Stokes drift into an additional source of TKE in the ML (see eqs. (4) and (5)). This also means that the effects of wave breaking and Langmuir production on TKE are not simply additive. Wave breaking modifies the shear near the surface, which in turn affects the Reynolds stresses, which in turn affect the Langmuir production of TKE.

2. – The influence of wave parameters on Langmuir effects

While LES studies [11, 7] have highlighted the importance of Langmuir circulations and their effects on the ML properties, a detailed exploration of the parameter space is still lacking. The authors in ref. [7] explored in great detail the LC effects for a mid-latitude (latitude $\varphi = 45°$) ML of depth $D = 33$ m, driven by a moderate wind (friction velocity $u_* = 0.0061$ ms^{-1}), for the case of a monochromatic surface gravity wave of 0.8 m amplitude and a wavelength $\lambda = 60$ m, traveling in the wind direction (angle $\alpha = 0$). Thus, the surface Stokes drift parameters were $V_{S0} = 0.068$ ms^{-1}, $La = 0.30$ and $kD = 3.47$.

Since eqs. (1) and (3) suggest that Langmuir input to TKE depends on the product of the ambient shear stress and the Stokes drift velocity, we define here an alternative Langmuir number named $Ln = \left(\frac{V_{S0}}{u_*}\right)^{1/3}$.

Ln and La are admittedly equivalent, the former having the advantage of increasing, unlike La, when V_{S0} increases; in the simulations presented by [7], $Ln = 2.24$. In ref. [5] it is showed that the two-equation second moment closure turbulence model of [8] simulated the case well [7], when eqs. (4) and (5) were employed with $E_6 = 7.2$. We use this model to explore the influence of the parameters Ln (or, equivalently, La) and kD on the ML properties. Additional details on the model structure can be found in [5]. We kept the ML depth D and friction velocity u_* unchanged (respectively, 33 m and 0.0061 ms^{-1}) but varied λ, φ, α and V_{S0}. Table I shows the different runs performed.

Figures 1 to 4 show profile results. Run 6 curve (stars) corresponds to the case of a wave running perpendicular to the prevailing wind stress, whereas Run 4 (circles) presents the case of a wave four times larger, and Run 3 (continuous thin line) that of a wave with a large wavelength (180 m). It can be seen that a wave running perpendicular to the wind (Run 6) distorts the Ekman spiral more than the wave running parallel to the wind (Run 1). It appears evident that the velocity profiles in the ML are significantly affected by the effect of LC. The influence can be large enough to distort the classical Ekman spiral in the mid- (and high-) latitude oceans (fig. 1), which may help explain why it has been difficult to discern the classical Ekman spiral in current measurements in the upper ocean. The larger the value of Ln (equivalently, smaller the value of La), the larger the distortion (compare Runs 4 and 5 with Run 0). In particular, the effect of LC on the surface velocity magnitude and direction with respect to the wind is extremely relevant. This is bound to have an impact on the drift of floating objects and spilled oil in the upper ocean.

TABLE I. – *Different run configurations.*

Run	u_* (m/s)	V_{S0} (m/s)	λ (m)	D (m)	Ln (La)	kD	φ (°)	α (°)	Description
0	0.0061	0	-	33	-	-	45	-	Standard Case (no LC)
1	0.0061	0.068	60	33	2.24 (0.3)	3.47	45	0	Standard Case (with LC)
2	0.0061	0.068	20	33	2.24 (0.3)	10.4	45	0	Reduced λ
3	0.0061	0.068	180	33	2.24 (0.3)	1.15	45	0	Increased λ
4	0.0061	0.272	60	33	3.55 (0.15)	3.47	45	0	Increased V_{S0}
5	0.0061	0.017	60	33	1.41 (0.6)	3.47	45	0	Decreased V_{S0}
6	0.0061	0.068	60	33	2.24 (0.3)	3.47	45	90	V_{S0} at 90^o to u_*
7	0.0061	0.068	60	33	2.24 (0.3)	3.47	0	0	Equatorial ML
8	0.0061	0.072	3.16	33	2.28 (0.29)	65.6	45	0	Li and Garrett [12]
9	0.0061	0.072	-	33	2.28 (0.29)	-	45	0	PM Spectrum
10	0.0061	0.072	-	33	2.28 (0.29)	-	45	0	Donelan Spectrum
11	0.0061	0.072	10.5	33	2.28 (0.29)	19.68	45	0	modified Li and Garrett

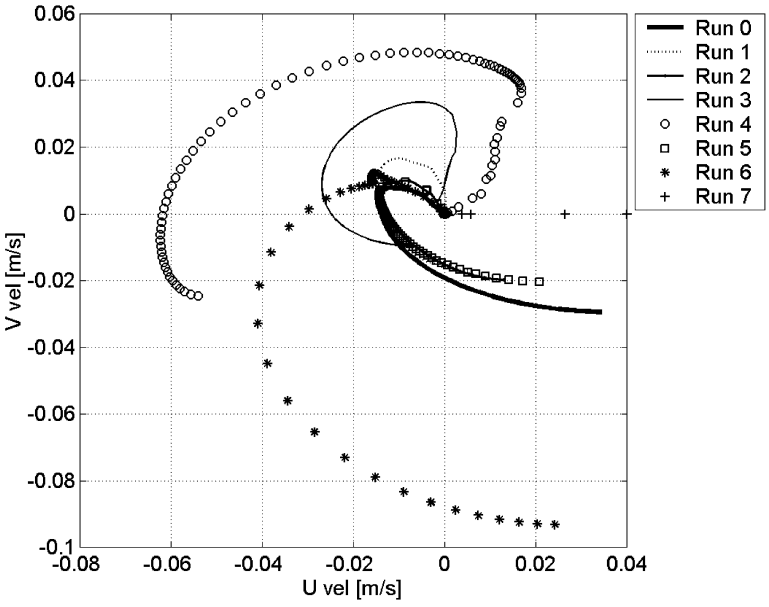

Fig. 1. – Hodograph showing the influence of LC on the ML velocities for different runs as listed in table I. The black thicker line denotes the reference run with no LC. The wind is along the horizontal axis and to the right.

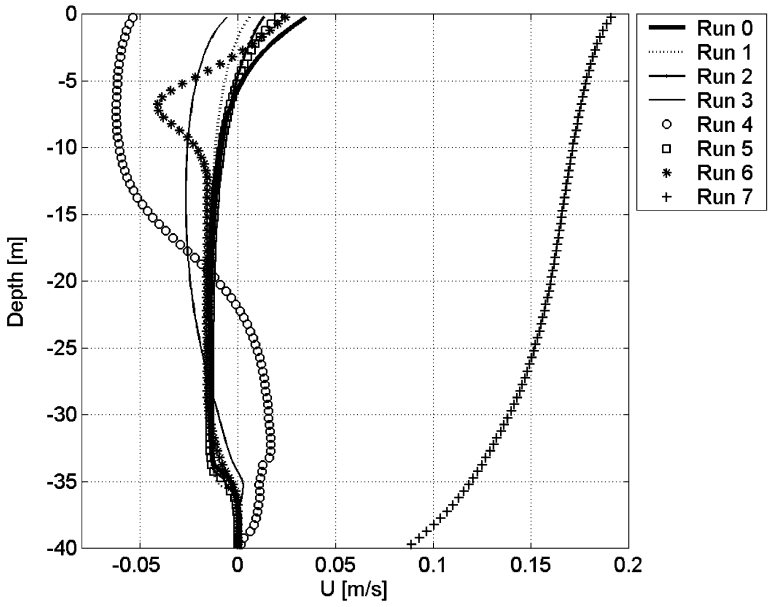

Fig. 2. – Profiles of U velocity (m/s) for different runs as listed in table I.

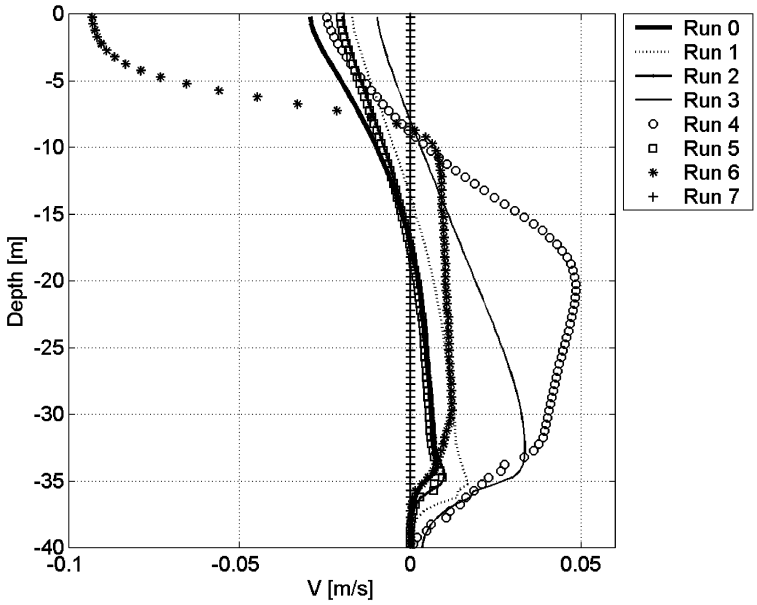

Fig. 3. – Profiles of V velocity (m/s) for different runs as listed in table I.

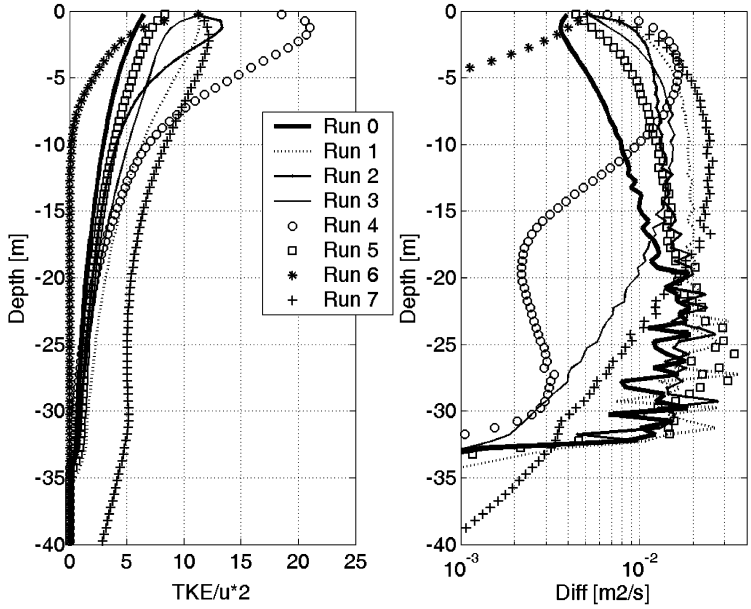

Fig. 4. – Profiles of TKE normalized by u_*^2 (left) and diffusivity (right) for different runs as listed in table I.

Generally speaking, including LC makes the velocities in the ML more uniform in the vertical (figs. 2 and 3). This is very much the result of increased mixing in the ML brought on by the Langmuir production terms in the turbulence equations. This enhancement of TKE (normalized by u_*) and of diffusivity can be seen in fig. 4 (respectively, left and right panel). It is worth noting that the three-dimensional effects of Langmuir circulation cannot be (and have not been) explicitly modeled. Nevertheless, the general behavior of the model is consistent with 3D LES simulations of LC turbulence in the upper ocean [7].

In the above simulations, the Stokes drift profile has been easily deduced from the properties of the incoming monochromatic wave. However, wind waves have a broad spectrum, and this means that the Stokes drift profile should be computed from the actual wave spectrum. To understand the influence of the spectral shape, we also ran the above simulations for the wind-wave spectra of "Pierson-Moskowitz" ([13], here called PM) and adopted in Run 9:

$$S(n) = (2\pi)^{-4}\,\alpha g^2 n^{-5} \exp\left[-1.25\left(\frac{n}{n_p}\right)^{-4}\right] \tag{6}$$

and "Donelan" [14], presented in Run 10:

$$S(n) = (2\pi)^{-4}\,\alpha g^2 n_p^{-1} n^{-4} \exp\left[-\left(\frac{n}{n_p}\right)^{-4}\right] \tag{7}$$

assuming that the wind wave spectrum is saturated. S is the frequency spectrum, n is the radian frequency, n_p is the frequency of the spectral peak, α is the Phillips parameter

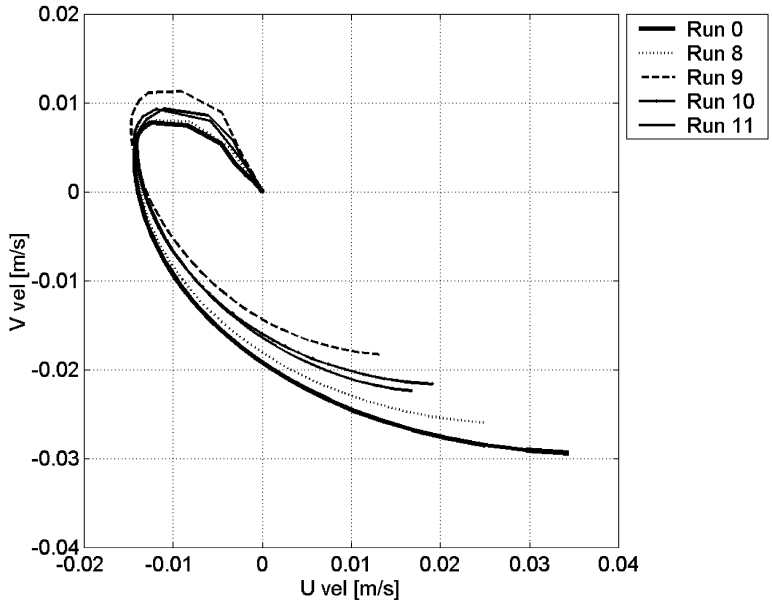

Fig. 5. – Hodograph for the same Langmuir number Ln of 2.28, but different values of the effective wave number, for different runs as listed in table I.

and g is the gravitational acceleration.

The Stokes drift profile was computed from

$$V_S(z) = \int_0^\infty \frac{n^3}{g} \exp\left[\frac{2n^2}{g} z\right] S(n) \mathrm{d}n \,. \tag{8}$$

In both cases, V_{S0} is proportional to U_{10} (or equivalently u_*) and equal to about 0.016 U_{10} (or 11.8 u_* assuming a value $C_d = 0.0015$), where U_{10} is the wind speed at 10 m. Thus, the Langmuir number $Ln\,(La)$ for a saturated wave field is about 2.28 (0.29), very close to [7] value. An equivalent wavelength is however hard to deduce. Li and Garrett [12] suggested an equivalent wavelength of $1.5(U_{10}^2/g)$ for a saturated wave field, which is used in Run 8. Figure 5 shows the resulting hodographs for Runs 8, 9 and 10, as well as for the case without LC (Run 0). Clearly, the [12] prescription underestimates the effect of the LC. If we assume that the Donelan spectrum approximates a saturated wind wave field reasonably well, a roughly similar result can be produced if the equivalent wavelength is assumed to be $5(U_{10}^2/g)$. The result from the modified Li and Garrett formulation is shown as Run 11.

Figures 6 and 7 show the corresponding vertical profiles of U and V velocity components, and fig. 8 the normalized TKE (left) and diffusivity (right) profile. It can be seen that Langmuir turbulence tends to enhance mixing and make velocity profiles more uniform in all the runs. In any case, the changes in the surface velocity magnitude and direction are significant enough that they ought to be taken into account in tracking floating or drifting objects in the upper ocean. If done so, the floating material such as spilled oil will drift with a slightly smaller velocity but more to the right with respect

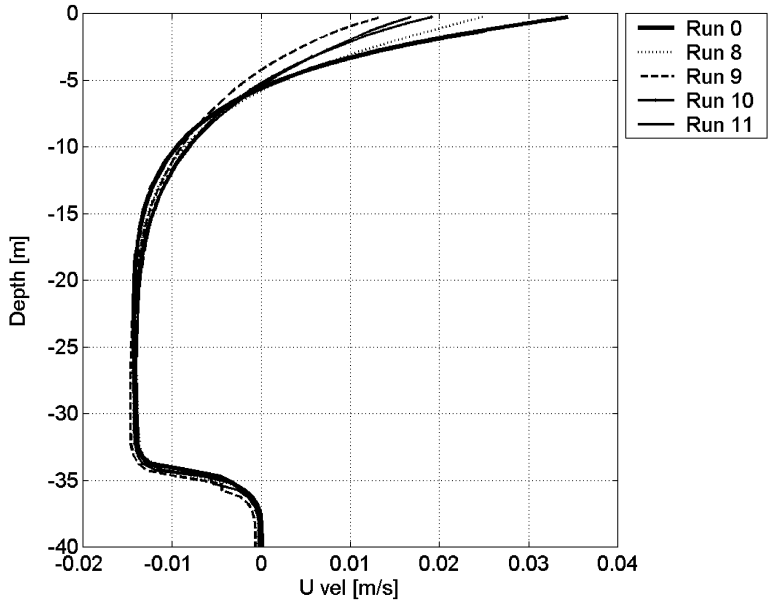

Fig. 6. – Profiles of U velocity (m/s) for different runs as listed in table I.

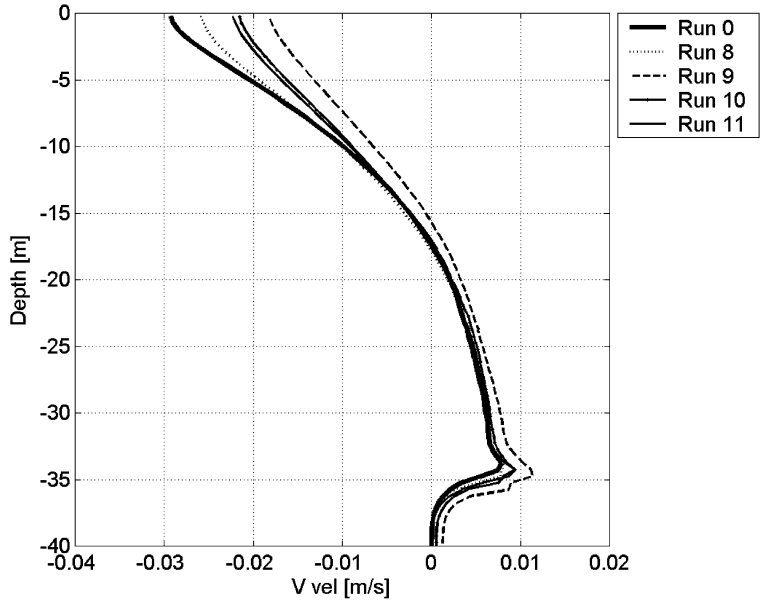

Fig. 7. – Profiles of V velocity (m/s) for different runs as listed in table I.

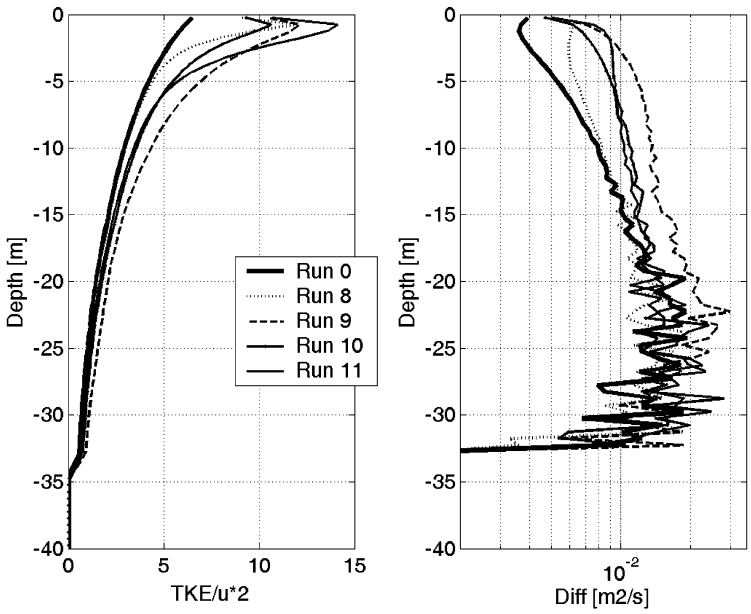

Fig. 8. – Profiles of TKE normalized by u_*^2 (left) and diffusivity (right) for different runs as listed in table I.

to the wind direction as can be seen by connecting the bottom points of the hodographs with the surface ones in fig. 1 and 5. Although operational wave forecasts are increasingly fulfilling this need, without *in situ* measurements the prevailing wind wave field cannot be known. However, in the absence of operational wave forecasts, it may be enough to assume that the waves are fully saturated and use the wind field resulting from operational forecasts to deduce the Stokes drift and account for the LC, at least approximately, using

$$(9) \qquad V_{S0} = 0.016 U_{10} \qquad \text{and} \qquad k = 1.25 \left(\frac{g}{U_{10}^2} \right) \qquad \left(\text{or} \quad \lambda = 5 \left(\frac{U_{10}^2}{g} \right) \right) .$$

To test the utility of eq. (9), the Stokes drift profile obtained using observed wave spectrum and the one resulting using the assumption of a saturated wave field (*i.e.* eq. (9) using measured U_{10}values) were compared, providing fairly consistent results (not shown here). Therefore, when the wave field information is not available, it is plausible to use eq. (9), which indeed will be used in the next section of the paper.

While the influence of LC on velocity structure and mixing is considerable, this does not always lead to a large influence on the MLT, since this is a strong function of the stratification prevailing in the water column.

In the above simulations, where the temperature below the ML is assumed to be linearly decreasing by $0.02\,^{\circ}\mathrm{C\ m^{-1}}$, the changes in the MLT due to the additional mixing from LC over the time span of the simulations (2 days) are less than $0.02\,^{\circ}\mathrm{C}$ (not shown). The changes in the MLT are due to air-sea heat transfer, as well as entrainment of colder waters from below the ML. Consequently, it is reasonable to expect more substantial changes when the ML is shallow and bounded by a weak thermocline. To explore these

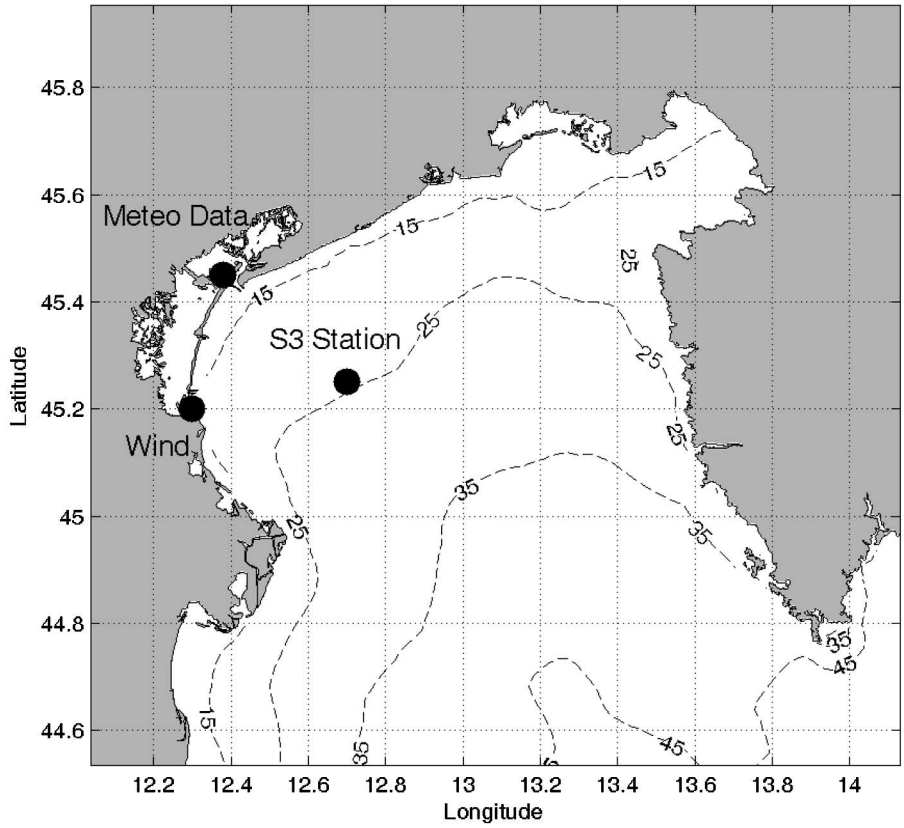

Fig. 9. – Location of the $S3$, wind and meteo stations in the north Adriatic basin. Some bathymetry lines are also shown.

aspects, we performed a simulation of the ML in the Northern Adriatic where a time series of ML properties and relevant meteorological forcings are available from a monitoring program carried out from 1999 to 2001.

3. – Model simulations in the Adriatic Sea

A two-year time series of observations are available at station $S3$ in the North Adriatic Sea (45.25° N, 12.70° E), close to the Venice lagoon, located in a water column 29 m deep (see fig. 9). The station was extensively monitored during the period 1999-2001 in the framework of the PRISMA-1 Project "Progetto di RIcerca per la Salvaguardia del Mare Adriatico" and INTERREG I-II [15] project. These campaigns enabled the collection of a wide variety of data, ranging from classic hydrographic to complex biogeochemical ones. From the physical point of view, the $S3$ area has usually been regarded as representative of the whole sub-basin [16]. This means that 1D simulations carried out here can be considered to yield water column properties that are a reasonable approximation to reality [17].

Temperature and salinity observations were carried out nearly every month at $S3$ using Hydronaut CTD. While no meteorological data were collected at the station itself

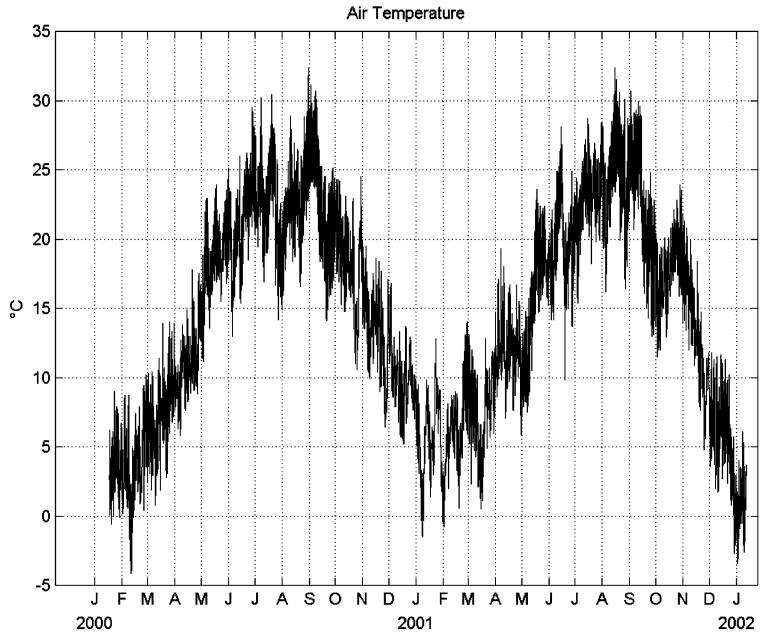

Fig. 10. – Hourly-averaged air temperature (in °C) as measured in Venice by the CNR-ISMAR during year 2000-2001.

before 2003, a complete set was available from an automatic weather registering station of CNR-ISMAR (formerly CNR, Istituto di Biologia del Mare) in Venice, about 30 km north from the station. The air temperature, atmospheric pressure, relative humidity and solar irradiance were collected every minute at the station, and the hourly averaged quantities used to derive the meteorological forcing needed by the model to simulate the seasonal evolution of the water column from January 17, 2000 to December 14, 2001. Since the winds registered at CNR-ISMAR underestimate the prevailing ones over the station, the wind speed and direction were obtained from a recording instrument in the proximity of Chioggia inlet (approximately 25 km SW of $S3$ station) run by the Centro Previsione Maree (CPM). Wind data were transformed into wind stress values assuming a wind-dependent drag coefficient; other effects (*e.g.*, atmospheric thermal stability) were considered as minor and therefore not included. The daily averaged value of cloud coverage, necessary to compute the net radiative heat flux, was obtained following the Reed formula [18] starting from year-day, latitude and measured solar insulation. The evolution of air temperature registered by the weather station during 2000-2001 is shown in fig. 10. The values are below 7 °C in January-February and increase to a maximum of about 30 °C in late summer. Six-hourly averaged wind magnitudes are shown in fig. 11: year 2000 values are presented in the upper panel, 2001 ones in the bottom one. Maximum values of wind intensity are reached during the end of June 2000, with hourly maxima up to 23 m s^{-1}, while the average intensity is about 4 m s^{-1}; dominant winds are mostly Bora, coming from N-E, and Scirocco, coming from S-E, while other winds occur with less probability.

Figure 12 shows the hourly-averaged total solar irradiance as measured by CNR-ISMAR, presenting the classic regional pattern with maximum values peaked during

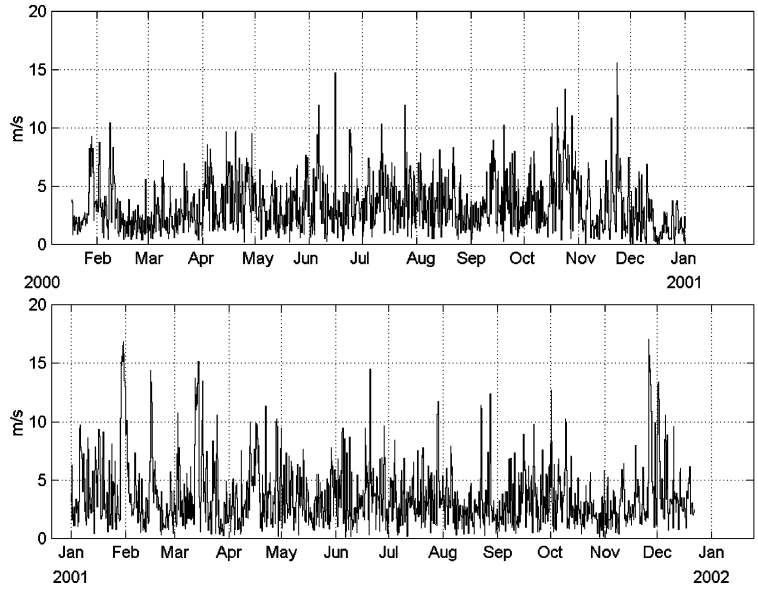

Fig. 11. – Six-hourly averaged wind speed (m s^{-1}) as measured in Chioggia by Centro Previsione Maree during 2000 (upper panel) and 2001 (lower panel).

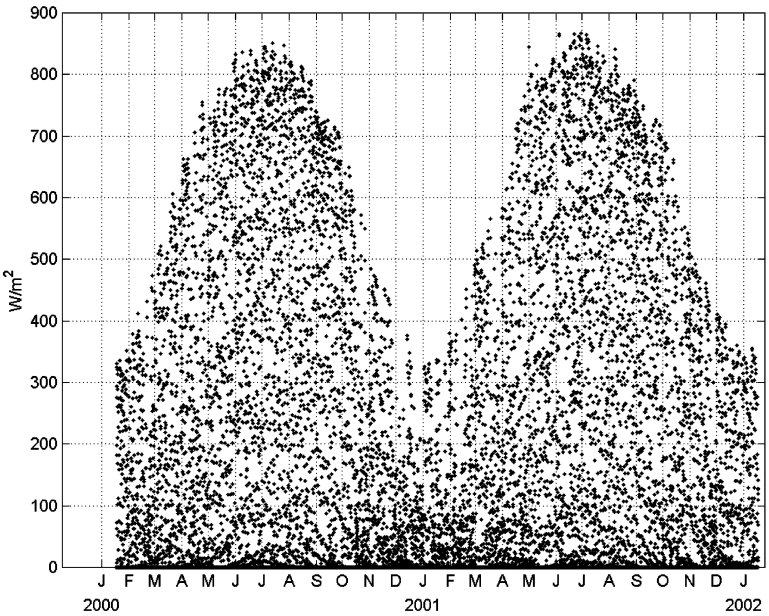

Fig. 12. – Hourly averaged solar irradiance (in W m^{-2}) as measured in Venice by CNR-ISMAR during year 2000-2001.

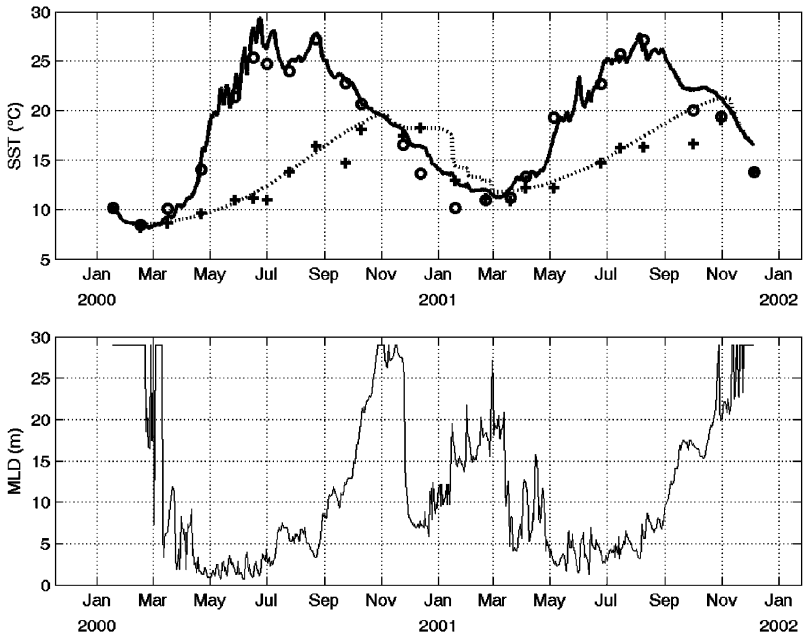

Fig. 13. – Upper panel: modeled surface (continuous) and bottom (dotted) temperatures, measurements (surface: circle; bottom: crosses). Lower panel: MLD evolution. Plots refer to year 2000-2001, standard case (no LC effect, no wave-breaking effects).

months from May to July, denoting a quasi-symmetric dome shape. The maximum value is reached at the beginning of June 2001, while the minimum one in late December 2000.

The 1D model deriving from eqs. (4) and (5) employed to simulate mixing at the Adriatic Station $S3$ has 29 levels along the vertical and an integration time step of 100 s; much higher resolution was adopted in test cases (up to 100 levels) without obtaining significantly different results. No assimilation techniques have been used on the temperature equation; on the other hand, since no reliable precipitation data were available, instead of computing the seasonal evolution of salinity in the ML, the values of this variable in the water column were assimilated using a simple nudging approach from observations. The equation of state was specified using the full UNESCO version [19]. Stokes drift parameters V_{S0} and k were assumed to correspond to the saturated wave field values and derived from wind stress data as described above (see eq. (9)). In order to validate model results, we extracted the 1 m depth-averaged CTD values, acquired around noon of each sampling day. The initial temperature profile used to initialize the model simulation is the January 2000 cast, which shows a completely-mixed water column at a temperature of about 10 °C.

The top panel of fig. 13 shows the modeled surface and bottom temperatures along with observed near-monthly values (surface observations denoted by circles; bottom ones by crosses), while the bottom panel presents the MLD during 2000-2001. Results are relative to the standard run, *i.e.* with no Langmuir and no wave-breaking effects. The curves show values without Langmuir effects at the surface (continuous line) and bottom (dotted line). The modeled SST is in good agreement with CTD observations, despite a slight overestimation in the spring-summer 2000 period. Specifically, the elevation of

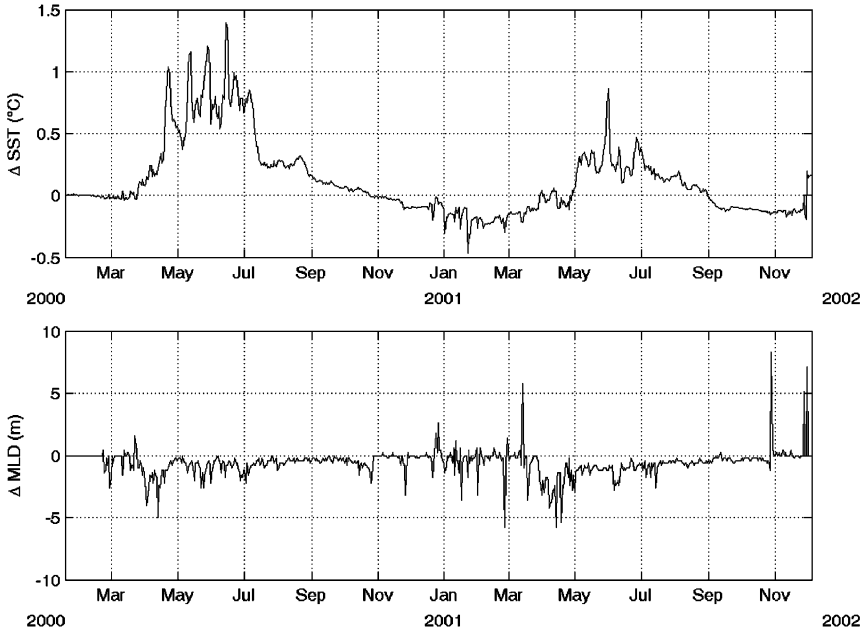

Fig. 14. – The differences in SST and MLD obtained between the standard run and the case with LC effect included.

bottom temperature to a value above that at the surface is clearly reproduced by the model.

Differences in SST and MLD between the standard case and the one including Langmuir effect are plotted in fig. 14. It can be seen that deviations are the largest during the spring/summer heating period when the ML is rather shallow. This is in accordance with [5] simulations at Station Papa in the North Pacific. The maximum difference in SST is around 1.4 °C (in ref. [5] a maximum SST difference of about 0.5 °C for station Papa was found), the differences occurring mostly between May and July. To show the relative importance of wave breaking, in fig. 15 we show the differences in SST and MLD between the standard run and that including only the wave-breaking effects. Both deviations in the SST and MLD structure, though being in the same direction as Langmuir effects, are smaller.

Figure 16 (upper panel) shows an expanded view for the year 2000, along with prevailing wind forcing in terms of magnitude (lower panel). Strong but brief bursts of wind stress can be seen to precede the decreases in SST, happening, as expected, when the ML is shallower and bounded by a weak thermocline. The dotted line presents the difference between the standard run and the wave-breaking one, the dashed line the difference between the standard case and the Langmuir-affected one, and the continuous line the difference between the reference run and when both Langmuir *and* wave-breaking effects are included. From this plot it appears that the combined effect is not purely given by the summation of the two separate effects (the pure sum is indeed slightly higher and most of the combined effect is due to Langmuir influence).

In general, however, while it is clear that the inclusion of Langmuir and wave-breaking turbulence produces in this application significant changes in SST (incidentally, these

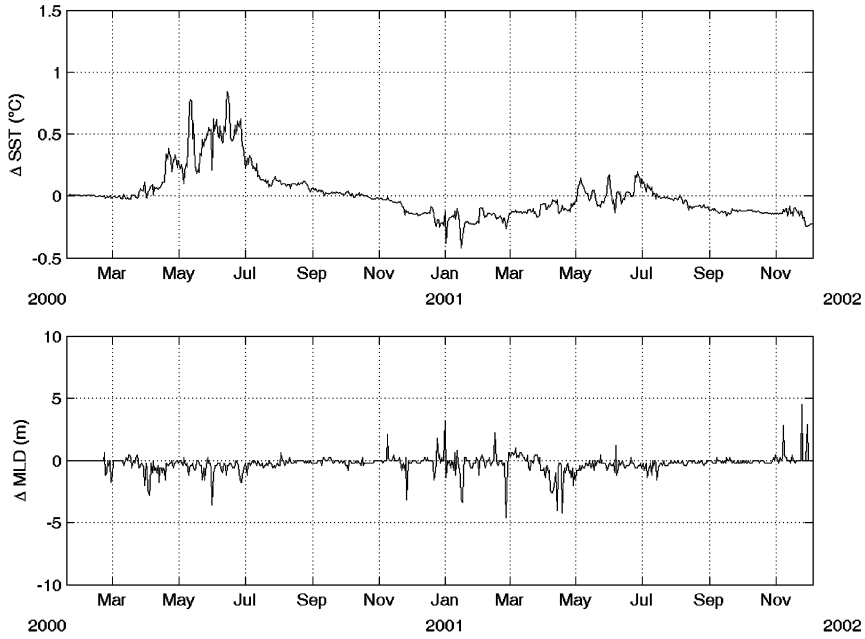

Fig. 15. – As in fig. 14, but showing now differences between the standard run and the case with only wave-breaking effects included.

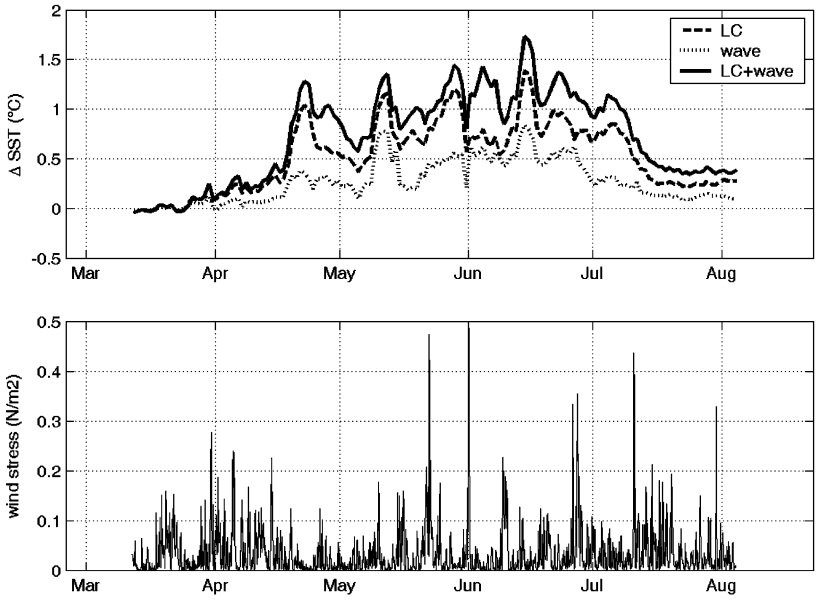

Fig. 16. – Upper panel: differences in SST during the year 2000 between the standard run and the wave-breaking one (dotted line), the LC effect one (dashed line), the run including both LC effects *and* wave breaking (continuous line). Lower panel: corresponding wind stress.

changes improve the agreement with data, as SSTs decreased with respect to the standard run in the spring-summer 2000 period), these changes are well within the uncertainties arising from uncertainties in the surface forcing. A small difference in the net air-sea heat flux or the magnitude of the wind forcing is capable of producing changes of similar magnitude. Moreover, the surface forcing can often be tuned slightly, well within known confidence limits, to yield results consistent with observations. When looking at the results shown in fig. 14, 15 and 16, this must be kept in mind.

4. – Idealized case studies

In an effort to understand the physical processes underlying the above results as well as to explore the parameter space of LC input, we performed several idealized case studies. There are several time scales of interest to mixing in the oceanic upper layers. The first is the storm timescale. Wintertime storm events bring about pronounced deepening of the ML on storm timescales of just a few days. The second is the diurnal timescale; daytime heating accompanied by nocturnal cooling modulates the MLD and MLT on this timescale. The effect is more pronounced during spring/summer heating period because of the higher solar insulation. Finally, there is the seasonal scale, when the MLT and MLD undergo seasonal evolution with shallow MLs and elevated SSTs during spring/summer heating period, and deep MLs and cooler SSTs during fall/winter cooling period. All three timescales are of interest in the study of mixing in the upper ocean.

4˙1. *Storm timescale.* – To test the influence of Langmuir TKE input on storm time scales, we initialized the model with stratification prevailing on day 110 of the two-year simulation. The prevailing wind stress on this day is 0.004 $\mathrm{Nm}^{-2}$and the ML is shallow (5 m, with MLD defined as the depth at which the temperature deviates 0.2 °C from the surface). We then increased the wind stress to 1.2 Nm^{-2} for half a day and ran the model with (Run $S1$) and without (Run $S0$) LC-driven turbulence using the modified Li and Garrett formulation (see again eq. (9)).

Figure 17 shows that the LC account for a drop in SST of about 0.6 °C occurring immediately after the increase in the wind stress magnitude. While this is less than the 1.5 °C change seen in the main run, the trend is right. Little differences in the results were evident when the increased stress was imposed for 1 and 2 days (not shown). Thus, we conclude that LC can amplify the drop in SST in an initially shallow ML brought on by a sudden increase of wind and, on storm timescales, LC can exert a non-negligible influence on the ML.

4˙2. *Diurnal timescale.* – One of the remarkable aspects of Langmuir circulation is their influence on very shallow diurnal MLs. Observations have repeatedly shown that the large diurnal buildup of MLT on a hot summer day, when the solar insulation is high and the winds low, can be wiped out completely by the passage of a strong swell through the area (see references cited in [20]). Under these conditions, the diurnal ML is very shallow, a few meters deep at best during the peak of solar insulation, but the heat gained during the day is distributed through the ML (bound by the seasonal thermocline a few tens of meters deep) during nocturnal cooling. This can lead to day/night-time SST differences of a few degrees in some cases. However, LC tend to deepen the diurnal ML and reduce these temperature differences. Part of their effect is undoubtedly the vertical transport induced by the cells. We cannot account for this in a 1D model, but part of the effect is due to TKE input from LC into the ML, and this latter part can be

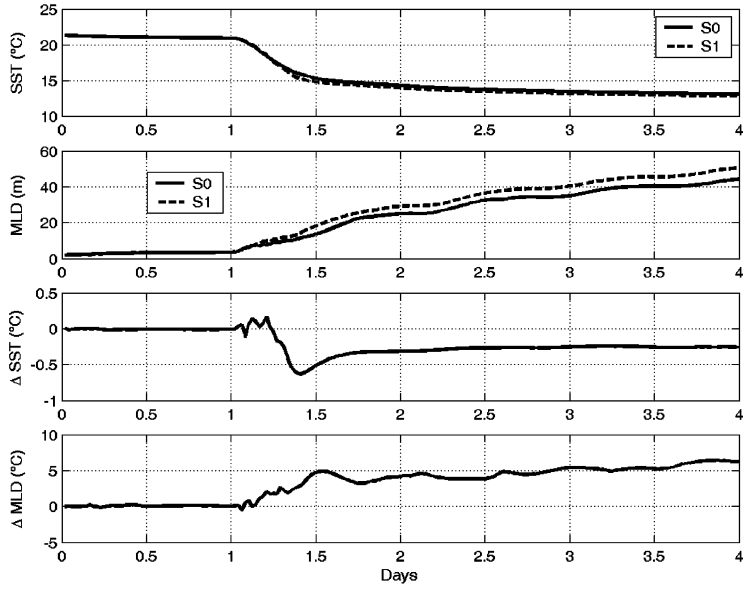

Fig. 17. – Evolution of SST, MLD and their differences in the case of standard run ($S0$) and including LC effect ($S1$). The plots refer to the case of a water column with a shallow ML affected by a sudden increase of wind (duration of half a day, from 0.004 to 1.2 Nm^{-2}).

simulated by a 1D model.

To assess the influence of this TKE input, we ran a few idealized experiments. The simulations were run with a water column depth of 100 m and uniform initial temperature of 28 °C in the upper 40 m. A strong thermocline was prescribed with a temperature drop of 3 °C with the stratification below being 0.1 °C/m. The peak solar insulation was 1000 Wm^{-2}, and the net outward air-sea flux was adjusted to make net heating over the day zero. Under these conditions, MLD is modulated between 5 m during the day to 35 m during the night and there is a corresponding modulation of SST.

Figure 18 shows the SST and MLD with and without the presence of a Stokes drift (wind stress 0.08 Nm^{-2}, $V_{S0} = 0.15$ ms^{-1}, wave traveling in the same direction as the wind, *i.e.* $\alpha = 0$, $\lambda = 60$ m, MLD = 40 m, $\varphi = 45°$). The diurnal modulation of the MLD is wiped out by the passage of the wave; however, since the diurnal ML is not very shallow, the change in SST is small, about 0.1 °C. Nevertheless, this illustrates the impact that LC may have on diurnal MLs, and fig. 19 depicts the effect on the Ekman spiral.

We tried to replicate the case of a shallow diurnal ML by choosing a diminished wind stress (0.004 Nm^{-2}, the rest of the setting is as above). This does produce a diurnal ML a few meters deep. However, the passage of a wave with a Stokes drift value of 0.1 ms^{-1} does not wipe out the diurnal modulation of SST, although the decrease is of the order of 0.2 °C (fig. 20). This is very likely due to the absence in the 1D model of vertical velocities induced by LC. In reality, the vertical transport induced by cellular circulation can transport surface water masses below the diurnal ML and hence wipe out the diurnal ML, and this effect is of course absent in a 1D model. It is worth noting, however, that the intense downward vertical velocities induced at the convergence zones of LC decrease

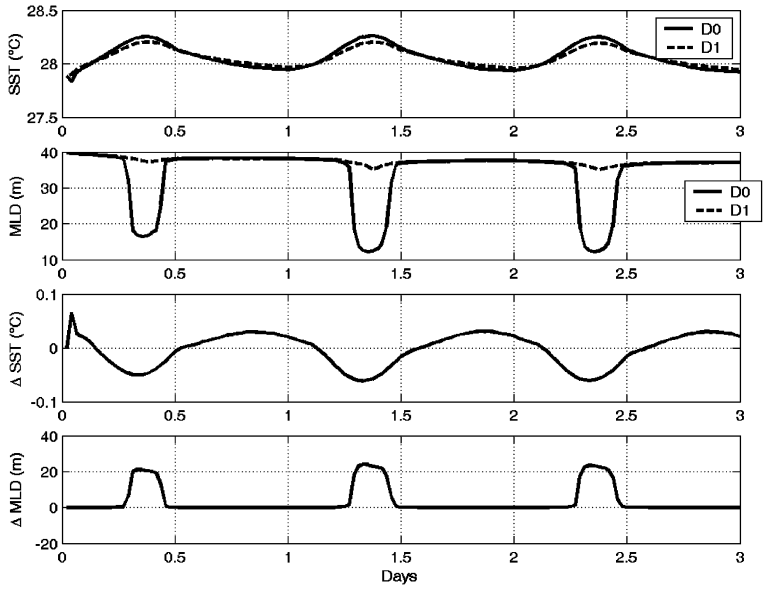

Fig. 18. – Case of a diurnal ML timescale. Evolution of SST, MLD and their differences in the case of standard run (D0) and including LC effect (D1).

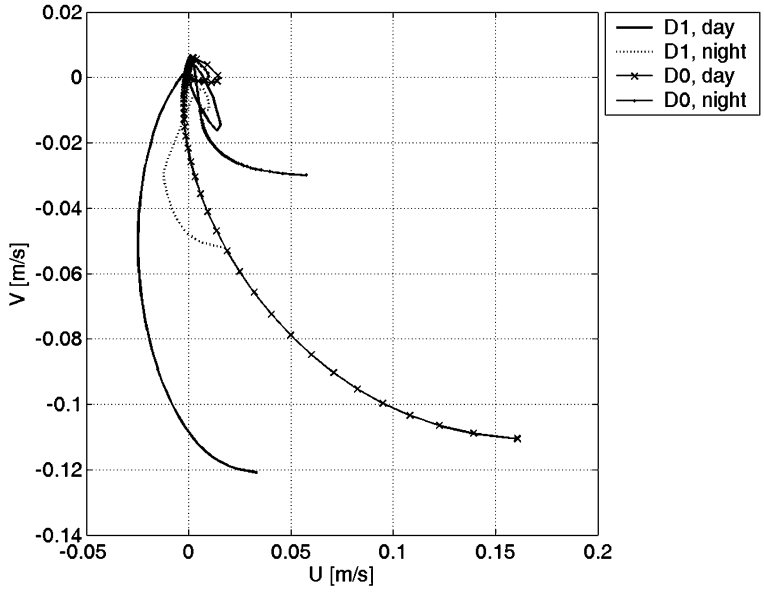

Fig. 19. – Hodographs referring to the case of a diurnal ML timescale, with (D1) and without (D0) LC turbulence. Both the day and night time spirals are shown.

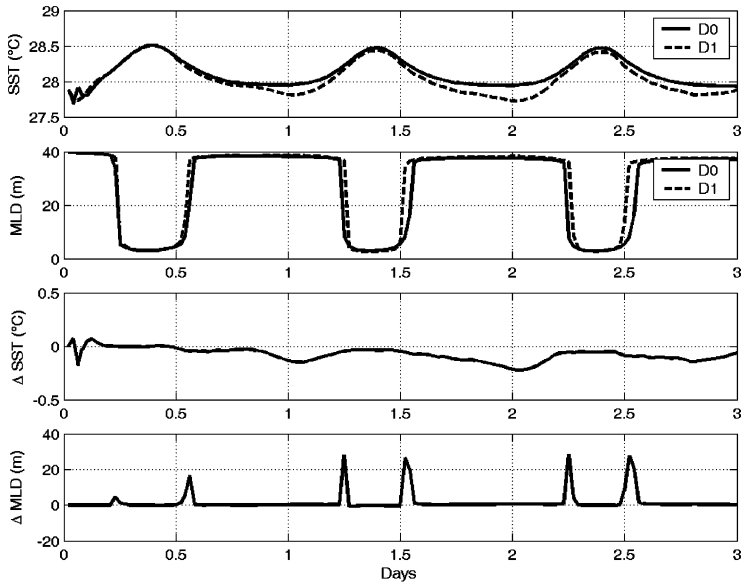

Fig. 20. – Evolution of SST, MLD and their differences in the case of standard run (D0) and including LC effect (D1). The plots refer to the case of a very shallow ML.

rapidly away from the surface and hence this model deficiency may not be particularly relevant when the ML is moderately deep, say a few tens of meters, as is the case on seasonal time scales.

Last, sensitivity studies were done to ascertain the influence of wave parameters on the diurnal ML. Figure 21 shows the standard case with (D1) and without (D0) LC (wind stress is 0.06 Nm^{-2}, Stokes drift value is 0.1 ms^{-1}, seasonal thermocline depth is 40 m). The maximum change in SST is 0.14 °C (peak to peak), not large, but not insignificant either. When the same wave runs perpendicular to the wind stress, the change is 0.3 °C. When the wavelength is reduced from 60 m to 20 m, the change decreases to 0.1 °C, whereas it remains pretty much unchanged at 0.13 °C when the wavelength is increased to 120 m. With a decrease in Stokes drift value to 0.06 ms^{-1}, the change decreases to 0.1 °C. Thus, the changes in the SST on diurnal time scales are confined to a few tenths of a degree, when the diurnal ML is not too shallow.

4˙3. *Seasonal timescale.* – The simulations in the Adriatic discussed above suggest that on seasonal scales, the inclusion of surface wave effects can result in SST differences of around 1 °C (see also Station Papa simulations analyzed by [5]). The effect is more pronounced during the spring/summer heating periods, when the ML is shallow. These differences are produced mainly during strong wind events, during which Langmuir TKE input into the ML causes increased deepening and hence lowering of the SST. Because the system has memory, this temperature difference can persist well beyond the season. Generally speaking, the differences are small during the fall/winter cooling periods, when the ML is rather deep.

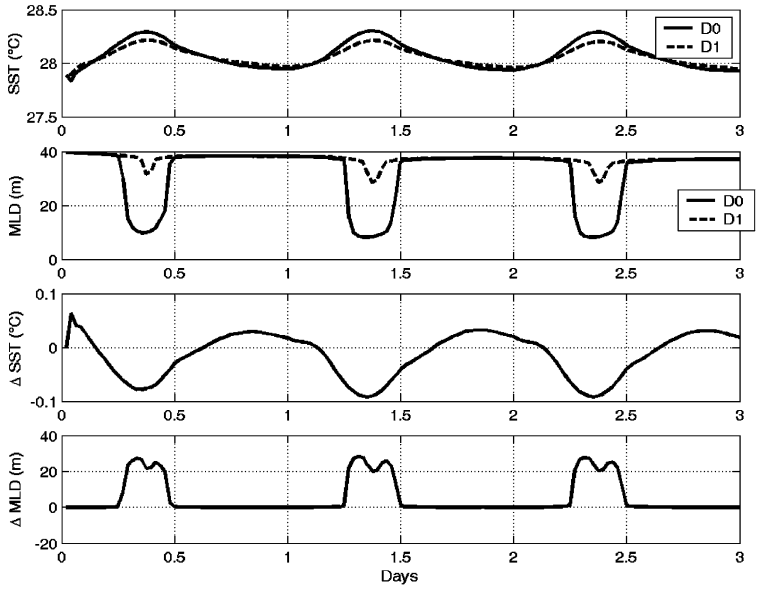

Fig. 21. – The reference case for sensitivity studies on wave parameters as described in the text, without (D0) and with (D1) LC effects.

5. – Concluding remarks

The modification of the mean momentum equations by LC through the introduction of an additional Coriolis term involving the Stokes drift, and the enhanced mixing due to LC-driven turbulence, modify significantly the ML velocity structure. The resulting Ekman spiral properties are therefore affected and this can have a considerable effect on the trajectories of drifting objects and spilled oil in the upper ocean.

The surface wave effects on the MLT depend on the time scale; while near-surface properties can be affected significantly by wave breaking, the changes in the bulk properties of the ML, especially when it is deep, tend to be small.

The effect of LC-driven turbulence on bulk properties is more significant. On diurnal time scales the changes seldom exceed 0.2 °C (note that the absence of cellular circulation in 1D models has a large impact on this result). On the other hand, during the passage of storms, the MLT can be depressed by as much as 0.5 °C, when the ML is shallow before the storm. On seasonal time scales, the effects can be cumulative and can add up to 1-2 °C during the spring/summer heating period, when once again the ML is shallow compared to the deep wintertime ones.

Nevertheless, the surface wave effects, which can be large under certain conditions, are generally within the errors introduced by uncertainties in external forcing of the models. This could explain why ML models, which have pretty much ignored surface wave effects until recently, have been reasonably depicting the evolution of the MLT at various timescales in spite of this omission.

* * *

We acknowledge with pleasure the support by ONR under grant ONR N00014-05-1-0730. The Italian authors were partially supported by the Project VECTOR (Italian

Ministry of University and Research—MIUR). SC expresses his gratitude to F. Botteon, S. Piovesana and T. Minuzzo for their precious help that allowed a fast data recovery. LHK thanks the ONR and Dr. M. Fladeiro for the partial support for this work through ONR grant N00014-03-1-0488. The support from the CNR-Short Term Mobility 2003-04 program and the hospitality of Venice CNR-ISMAR during his visit and work on this paper is also acknowledged with pleasure.

REFERENCES

[1] Mellor G. L., *J. Phys. Oceanogr.*, **33** (2003) 1978.
[2] Ardhuin F. and Jenkins A. D., to be published in *J. Fluid Mech.* (2005) http://arxiv.org/abs/physics/0504097.
[3] Kantha L. H., *Ocean Modelling*, **11** (2006) 167.
[4] Burchard H., *J. Phys. Oceanogr.*, **31** (2001) 3133.
[5] Kantha L. H. and Clayson C. A., *Ocean Modelling*, **6** (2004) 101.
[6] Craik A. D. D. and Leibovich S., *J. Fluid Mech.*, **73** (1976) 401.
[7] Mcwilliams J. C., Sullivan P. P. and Moeng C. H., *J. Fluid Mech.*, **334** (1997) 1.
[8] Kantha L. H. and Clayson C. A., *J. Geophys. Res.*, **99** (1994) 25235.
[9] Burchard H. and Baumert H., *J. Geophys. Res.*, **100** (1995) 8523.
[10] Carniel S., Kantha L. H. and Sclavo M., *Ann. Hydrograph.*, **3**, n. 772 (2004) 8-1.
[11] Skyllingstad E. D. and Denbo D. W., *J. Geophys. Res.*, **100** (1995) 8501.
[12] Li M. and Garrett C., *J. Mar. Res.*, **51** (1993) 737.
[13] Pierson W. J. and Moskowitz L., *J. Geophys. Res.*, **69** (1964) 5181.
[14] Donelan M. A., Hamilton J. and Hui W. H., *Philos. Trans. R. Soc. London, Ser. A*, **315** (1985) 509.
[15] Rabitti S. *et al.*, *Archo Oceanogr. Limnol.*, **23** (2002) 130.
[16] Zavatarelli M. *et al.*, *J. Mar. Syst.*, **18** (1998) 227.
[17] Vichi M. *et al.*, *Ann. Geophys.*, **21** (2003) 413.
[18] Reed R. K., *J. Phys. Oceanog.*, **7** (1977) 482.
[19] Gill A. E., *Atmosphere-Ocean Dynamics* (Academic Press) 1982, p. 662.
[20] Kantha L. H. and Clayson C. A., *Small Scale Processes in Geophysical Flows* (Academic Press) 2000, p. 888.